A Covalent Linker Allows for Membrane Targeting of an Oxylipin Biosynthetic Complex[†,‡]

Nathaniel C. Gilbert, Marc Niebuhr, Hiro Tsuruta, Tee Bordelon, Oswin Ridderbusch, Adam Dassey, Alan R. Brash, Sue G. Bartlett, and Marcia E. Newcomer*

Department of Biological Sciences, Louisiana State University, Baton Rouge, Louisiana 70803

Received April 28, 2008; Revised Manuscript Received July 28, 2008

ABSTRACT: A naturally occurring bifunctional protein from *Plexaura homomalla* links sequential catalytic activities in an oxylipin biosynthetic pathway. The C-terminal lipoxygenase (LOX) portion of the molecule catalyzes the transformation of arachidonic acid (AA) to the corresponding 8*R*-hydroperoxide, and the N-terminal allene oxide synthase (AOS) domain promotes the conversion of the hydroperoxide intermediate to the product allene oxide (AO). Small-angle X-ray scattering data indicate that in the absence of a covalent linkage the two catalytic domains that transform AA to AO associate to form a complex that recapitulates the structure of the bifunctional protein. The SAXS data also support a model for LOX and AOS domain orientation in the fusion protein inferred from a low-resolution crystal structure. However, results of membrane binding experiments indicate that covalent linkage of the domains is required for Ca^{2+}-dependent membrane targeting of the sequential activities, despite the noncovalent domain association. Furthermore, membrane targeting is accompanied by a conformational change as monitored by specific proteolysis of the linker that joins the AOS and LOX domains. Our data are consistent with a model in which Ca^{2+}-dependent membrane binding relieves the noncovalent interactions between the AOS and LOX domains and suggests that the C2-like domain of LOX mediates both protein−protein and protein−membrane interactions.

The ability of the cell to respond to its environment is dependent upon effective coordination of metabolic pathways. For those pathways that involve the biosynthesis of the arachidonic acid (AA)[1] derived lipid mediators such as the leukotrienes, prostaglandins, and thromboxanes, their coordination may be exceptionally challenging in terms of substrate acquisition and specificity. The hydrophobic substrates partition into the membrane phase, and active sites that recognize bulky hydrophobic compounds might be inherently promiscuous. Furthermore, the highly reactive fatty acid hydroperoxide intermediates promote cellular oxidative damage if their metabolism is not stringently regulated. Both compartmentalization of enzymes and organization of multienzyme complexes are thought to provide cellular mechanisms for "traffic control" in pathways for the synthesis of these potent signaling molecules (*1*−*3*). In order to understand how coordination of biosynthetic pathways is achieved in the context of cell trafficking, and specifically how facilitated transfer of intermediates between active sites might be a means to regulate pathway flux, we have focused our efforts on an eicosanoid biosynthetic enzyme that contains both 8*R*-lipoxygenase (8*R*-LOX) and allene oxide synthase (AOS) activities in a naturally occurring fusion protein.

Lipoxygenases, which catalyze the regio- and stereospecific dioxygenation of polyunsaturated fatty acids (*4*−*6*), are composed of two domains: an amino-terminal β-barrel domain and a largely α-helical catalytic domain (*7*−*12*). The amino-terminal domain of lipoxygenase resembles a C2 domain, the calcium-dependent membrane-binding module found in phospholipases and kinases (*13, 14*), and is referred to as the C2-like domain. The structure of the independently

[†] This work was supported in part by the National Science Foundation (MCB-0818387), the Louisiana Governor's Biotechnology Initiative (MEN), and the National Institutes of Health (GM 074888 to A.R.B.). Portions of this research were carried out at the Stanford Synchrotron Radiation Laboratory, a national user facility operated by Stanford University on behalf of the U.S. Department of Energy, Office of Basic Energy Sciences. The SSRL Structural Molecular Biology Program is supported by the Department of Energy, Office of Biological and Environmental Research, and by the National Institutes of Health, National Center for Research Resources, Biomedical Technology Program Grant 5 P41 RR001209. The contents of this work are solely the responsibility of the authors and do not necessarily represent the official view of NCRR or NIH. Diffraction data used in this publication were collected at the Gulf Coast Protein Crystallography (GCPCC) Beamline at the Center for Advanced Microstructures and Devices (CAMD). This beamline is supported by National Science Foundation Grant DBI-9871464 with cofunding from the National Institute for General Medical Sciences (NIGMS).

[‡] Coordinates for the crystal structure have been deposited in the Protein Data Bank (accession code 3DY5).

* Author to whom correspondence should be addressed. Tel: (225) 578-7383. Fax: (225) 578-7258. E-mail: newcomer@lsu.edu.

[1] Abbreviations: arachidonic acid, AA; allene oxide, AO; lipoxygenase, LOX; 8*R*-hydroperoxyeicosatetraenoic acid, 8*R*-HPETE; phosphatidylcholine, PC; phosphatidylserine, PS; fluorescence resonance energy transfer, FRET; 1,2-dihexadecanoyl-*sn*-glycero-3-phosphoethanolamine, DHPE; 1-stearoyl-2-arachidonyl-*sn*-glycero-3-phosphatidylcholine, AA-PC; tobacco etch virus, TEV; large unilamellar vesicles, LUV; *N*-(1-pyrenesulfonyl)-1,2-dihexadecanoyl-*sn*-glycero-3-phosphoethanolamine, pyS-DHPE; *N*-(5-dimethylaminonaphthalene-1-sulfonyl)-1,2-dihexadecanoyl-*sn*-glycero-3-phosphoethanolamine, dansyl-DHPE; AOS-TEVsite-LOX fusion protein, TEV-FP; LOX + AOS heterodimer, HD; LOX-AOS fusion protein, FP; small-angle X-ray scattering, SAXS; size exclusion chromatography, SEC.

10.1021/bi800751p CCC: $40.75
Published on Web 09/12/2008

expressed 8*R*-LOX domain of the fusion protein revealed clearly defined calcium binding sites in its C2-like domain, and fluorescence data indicated that Ca^{2+}-binding amino acids are required for membrane binding. A double mutant in which amino acids in two of the Ca^{2+} sites are mutated does not bind membranes but has wild-type activity in a membrane-free assay (*11*). In addition, a deletion mutant lacking a putative C2-like domain membrane-insertion loop common to 8*R*- and 5-LOX (but absent in 15-LOX) has wild-type activity in a membrane-free assay but is impaired with respect to membrane binding: enzyme activity is not stimulated by Ca^{2+} when assayed in the presence of liposomes (*15*). In the context of the naturally occurring fusion protein, the C2-like domain is flanked by the N-terminal AOS domain and the C-terminal LOX catalytic domain. The structure of the independently expressed AOS domain has also been reported (*16*). *Plexaura homomalla* AOS structurally resembles catalase, both in terms of the polypeptide fold and the constellation of amino acids that constitute the heme environment.

Early studies of oxylipin biosynthesis in the soft coral *P. homomalla* led to the identification of an activity in the microsomal fraction (*17*) that was subsequently attributed to the bifunctional 8*R*-LOX-AOS fusion protein (*18*). The product of the two activities is now considered a likely precursor of marine prostanoid derivatives such as the clavulones (*19*−*21*). The bifunctional coral enzyme, or "fusion protein", catalyzes successive steps in an eicosanoid biosynthetic pathway: the transformation of arachidonic acid to 8*R*-hydroperoxyeicosatetraenoic acid (8*R*-HPETE) by the 8*R*-LOX domain and the subsequent conversion of the intermediate to the corresponding allene oxide by the AOS domain. It has been postulated that when two interacting proteins are fused, successive mutations will eventually create an optimized protein−protein interface (*22*). Thus, it is predicted that fusion proteins, when expressed independently, should associate *via* these optimized protein−protein interfaces. Furthermore, what occurs as a fusion protein in one species may be found as a complex of multiple polypeptides in another (e.g., fatty acid synthase), and thus the existence of a fusion protein in an organism may be indicative of interacting proteins in other organisms (*22*).

We investigated the function of the covalent linkage of the AOS and LOX activities and present evidence that the independently expressed domains associate in the absence of the covalent linker. Small-angle X-ray scattering experiments reported herein demonstrate that a chromatographically purified complex of AOS and 8*R*-LOX (heterodimer, HD) recapitulates the solution structure of the full-length fusion protein (FP). Furthermore, SAXS data are consistent with one of two models for AOS and 8*R*-LOX domain association inferred from a low-resolution crystal structure of the fusion protein. However, membrane-binding experiments indicate that covalent linkage of the individual enzymatic domains is required for Ca^{2+}-dependent membrane targeting of the sequential catalytic activities. Limited proteolysis and membrane binding experiments with FP suggest that Ca^{2+}-dependent membrane binding is accompanied by a conformational change that releases AOS from noncovalent interactions with the LOX domain. The construction of a mutant form of the naturally occurring fusion protein in which a tobacco etch virus (TEV) protease cleavage site is positioned between the AOS and LOX domains allowed us to distinguish conformational states of FP that differ in access to the TEV-protease site. Taken together, our observations suggest that the covalent linker that links the LOX and AOS domains in FP is required to compartmentalize the sequential catalytic activities at the membrane.

EXPERIMENTAL PROCEDURES

Construction of the Native AOS-LOX Fusion Protein Expression Plasmid. Plasmids containing the genes for the AOS and lipoxygenase domains of FP were used as templates to amplify the genes for each by polymerase chain reactions (PCR). The native AOS-LOX fusion protein was reconstructed by overlap extension PCR. First, the lipoxygenase gene was PCR-amplified using a forward primer designed to anneal at the beginning of the coding sequence and a reverse primer having a 5′ *Bam*HI restriction site for subsequent cloning. Next, the AOS gene was PCR-amplified using a forward primer containing a 5′ *Nde*I restriction site and a reverse primer that anneals to the last 19 nucleotides of the AOS gene and has a 5′ extension containing 22 additional nucleotides that are complementary to the first 22 nucleotides of the LOX gene. Both amplicons from the above PCR reactions were then combined, and overlap PCR was done in which the 22 nucleotide overlap amplicons were allowed to anneal and serve as the primers for DNA polymerase extension to create the gene for the full-length AOS-LOX fusion protein. Included in the overlap PCR reaction was the AOS forward primer and the LOX reverse primer so that amplification of the full-length AOS-LOX gene would proceed. The full-length AOS-LOX DNA was gel-purified and cloned into pSTBlue-1 (Novagen) at the *Eco*RV site. An *Nde*I/*Bam*HI digestion excised the AOS-LOX gene which was then ligated into pET28 (Novagen) digested with the same enzymes. The resulting expression plasmid, pTBfusion, expresses the fusion protein under control of an isopropyl β-D-thiogalactopyranoside (IPTG) inducible T7 promoter. Plasmid pTBfusion was sequenced to confirm that no point mutations had occurred during PCR and to verify that the junction between the AOS and LOX genes maintained the correct reading frame required to yield the native FP.

Construction of AOS-TEVsite-LOX Fusion Protein Expression Plasmid. The AOS/TEVsite/LOX fusion was assembled in pLITMUS 28i (New England Biolabs) as follows. The AOS sequence encoding amino acids 1−367 of FP was amplified by PCR using a 5′ primer containing a *Kpn*I site and a 3′ primer containing an *Avr*II site. The PCR product was digested with *Avr*II and *Kpn*I and cloned into pLITMUS 28i digested with the same enzymes. The sequence encoding the 8*R*-LOX portion of FP (from amino acid 373 to the stop codon) was amplified using a 5′ primer containing an *Age*I site and a 3′ primer containing a *Bam*HI site. The PCR product was digested with *Age*I and *Bam*HI and cloned into AOS/pLITMUS digested with the same enzymes.

The TEV cleavage site was constructed using synthetic oligonucleotides containing a *Spe*I overhang at the 5′ end and an *Age*I overhang at the 3′ end. This linker was cloned into AOS-8*R*-LOX/LITMUS digested with *Avr*II and *Age*I. The resulting chimeric protein, AOS-TEVsite-8*R*-LOX (TEV-FP), contains the sequence PSENLYFQGTG between amino

acids 367 and 373 of the original fusion protein. The AOS-TEVsite-8*R*-LOX sequence was excised from LITMUS 28i using *Nde*I and *Bam*HI and cloned into pET28b digested with the same enzymes. This construct was transformed into *Escherichia coli* BL21(DE3) cells for expression.

Protein Expression and Purification. The individually expressed LOX and AOS domains were purified as previously described (*11, 16*). FP was purified from an *E. coli* expression system. BL21(DE3) cells carrying pTBfusion were grown in Terrific Broth at 37 °C until the A_{600} exceeded 0.6, at which time the temperature was reduced to 18 °C. After 26 h at this temperature the cells were harvested, pelleted by centrifugation, and frozen at −80 °C. Cell pellets were resuspended in Bugbuster (Novagen) according to the manufacturer's instructions, and the protease inhibitors pepstatin and leupeptin were added. After the addition of DNase I (Sigma-Aldrich), the suspensions were sonicated. Cell debris was removed by centrifugation, and the supernatant was applied to Ni-NTA agarose (GE Healthcare) in 10 mM Tris (pH 8) and 500 mM NaCl (buffer A). The column was washed with 10 mM buffer A supplemented with 20 mM imidazole and subsequently eluted with an imidazole gradient (20−200 mM in buffer A). The fractions containing FP had absorbance maxima at 280 and 406 nm. Further purification on Mono-Q (20 mM Tris, pH 8, 0−500 mM NaCl) and Superdex-200 size exclusion chromatography (SEC) columns (GE Healthcare) (10 mM Tris, pH 8, 150 mM NaCl) yielded pure enzyme as judged by SDS−PAGE and the ratio of A_{280} to A_{406}. To ensure full heme substitution in the AOS domain, excess heme was added prior to application of the sample to the Superdex-200 column. TEV-FP was expressed and purified according to the protocol for native FP.

Size Exclusion Chromatography. For preparative scale LOX + AOS heterodimer (HD) isolation, independently purified LOX and AOS domains were mixed and applied to a Superdex-200 (GE Healthcare) column mounted on an ÄKTA FPLC. Analytical runs to monitor complex formation were performed with a Bio-Rad Biologics FPLC fitted with Pharmacia Superose-12 column buffered with 20−50 mM Tris (pH 7.5) and 150 mM NaCl at a flow rate of 1 mL/min. In this system, the complex elutes at 12.5 mL and free AOS (as a dimer) elutes at 13.5 mL. Protein elution is simultaneously monitored at 280 and 406 nm with a Bio-Rad Quadtec detector. Absorbance at 406 nm is due to the AOS heme. HD has 1 heme for 1066 amino acids, and the absorbance at 280 nm is greater than that at 406 nm. The reverse is true for AOS, which has 1 heme for 373 amino acids.

Small-Angle X-ray Scattering Data. SAXS data were collected at SSRL beamline 4-2 (*23*) for both FP and HD purified by size exclusion chromatography. HD and FP were concentrated to 10 mg/mL in Centricon-50 (Millipore) centrifugal filter devices. SAXS measurements were taken at concentrations ranging from 1 to 10 mg/mL. The sample-to-detector distances of 1.0 and 2.5 m were used to cover the Q range 0.01−0.3 Å^{-1}, where Q is the momentum transfer $4\pi \sin(\theta)/\lambda$ with θ and λ being the half-scattering angle and the wavelength, respectively. The double crystal monochromator was calibrated to give the X-ray beam energy of 9 keV. A MarCCD165 detector was used throughout the measurements, and detector pixel numbers were calibrated to corresponding Q values by the (100) and related higher order reflections of silver behanate powder sample placed at the sample position. All samples contained 20 mM Tris (pH 8.0) and 150 mM NaCl. A 30 μL sample aliquot was loaded into the quartz capillary cell maintained at 20 °C and continuously moved in the beam at 1 μL/s by a computer-controlled syringe pump during the X-ray exposure to minimize radiation damage. A series of ten data frames with 15 s exposure each were recorded for the sample aliquots. Blu-ICE/DCS and MarParse programs were used for data collection and processing, respectively (*23*). The radii of gyration and forward scattered intensities $I(Q = 0)$ were calculated with Primus (*24*). The electron pair distance distribution function was computed by running Gnom, an indirect Fourier transform program (*25*). The SAXS experiments were repeated with the addition of 2 mM $CaCl_2$ for both FP and HD. LOX and AOS scattering curves were calculated from their crystal structures (monomeric LOX and dimeric AOS) with Crysol (*26*), which takes into account a hydration layer. The calculated scattering intensities of LOX and dimeric AOS were arithmetically summed at each Q value to simulate a scattering curve that would be expected for a simple mixture without forming a complex. Crysol was also used to obtain scattering curves for the two possible conformations of fusion protein inferred from a low-resolution crystal structure. The structures of the independently determined AOS and 8*R*-LOX structures docked according to the 3.5 Å crystal structure were used for these calculations.

Crystal Structure Determination. FP crystals were obtained by the hanging-drop vapor diffusion method with drops prepared with 2:1:1 mixtures of FP (5 mg/mL in 4 mM $CaCl_2$), detergent (1.8 mM Triton X-100), and precipitant (16% PEG 3350, 4% Tacsimate, pH 6.0) at 22 °C. Thin plate crystals in the monoclinic space group $C2$ (a = 235.5 Å, b = 77.5 Å, c = 158.0 Å, β = 112.5°) diffract to 3.5 Å. Diffraction data were collected at the protein crystallography beamline at the Center for Advanced Microstructures and Devices at Louisiana State University on a MarCCD165 detector at 100 K. Indexing, integration, and scaling were done with HKL2000 (*27*). The structure was solved by molecular replacement with MOLREP in the CCP4 suite (*28*) of programs. Due to noncrystallographic symmetry (NCS), there are two molecules in the asymmetric unit. A multicopy search with 2.0 Å resolution models of both AOS (1U5U) and an 8*R*-LOX deletion mutant (ref *15*; Neau et al., unpublished) positioned two monomers of each in the asymmetric unit. After multiple cycles of manual rebuilding followed by translation, libration and screw rotation (TLS), and NCS-restrained refinement in REFMAC5 (*28*), the model included residues 3−367 of the AOS domain and residues 373−410, 418−447, 450−567, 599−677, 688−951, and 959−1066 of the LOX domain (R_{work}/R_{free} 27.3/32.2). At this point, electron density was visible in a $2|F_o - F_c|$ map contoured at 1σ that, with a single short break, connects the C-terminus of an AOS module to the amino terminus of LOX. This density accommodates the linker region that joins the AOS and LOX domains as required for the SAXS-supported model. Data and refinement statistics are provided in Table 1.

Liposome Preparation. Large unilamellar vesicles were prepared from a mixture of porcine brain phosphatidylcholine

Table 1: X-ray Data Processing and Refinement Statistics[a]

Data Collection	
space group	*C*2
cell parameters	232.5, 77.5, 158.0 Å $\beta = 112.5°$
wavelength (Å)	1.38
resolution (Å)	40−3.51 (3.63−3.51)
unique reflections	32749 (2833)
completeness (%)	98.3 (86.8)
redundancy	3.4 (2.6)
R_{merge}	0.135 (0.364)
$\langle I/\sigma(I)\rangle$	8.5 (1.8)
Refinement	
resolution (Å)	20.86−3.51
reflections	30961
σ cutoff	none
no. of atoms	
protein	16130
ligand	88
R_{work}	0.273
R_{free}	0.320
rmsd from ideal geometry	
bond length (Å)	0.010
bond angle (deg)	1.23

[a] Values for the highest resolution shell are given in parentheses. $R_{merge} = \sum_{hkl}[(\sum_j|I_j - \langle I\rangle|)/\sum_j|I_j|]$; $R_{work} = \sum_{hkl}||F_o| - |F_c||/\sum_{hkl}|F_o|$, where F_o and F_c are the observed and calculated structure factors, respectively. R_{free} is computed for 5% randomly selected reflections omitted from the refinement.

(PC) and phosphatidylserine (PS) in 3:1 molar ratio (LUV) or with 1-stearoyl-2-arachidonyl-*sn*-glycero-3-phosphatidylcholine (AA-PC) and porcine brain PS in a 3:1 molar ratio (AA-LUV). All phospholipids were purchased from Avanti Polar Lipids. For LUVs that incorporated fluorescent labels, either *N*-(1-pyrenesulfonyl)-1,2-dihexadecanoyl-*sn*-glycero-3-phosphoethanolamine (pyS-DHPE; Molecular Probes) or *N*-(5-dimethylaminonaphthalene-1-sulfonyl)-1,2-dihexadecanoyl-*sn*-glycero-3-phosphoethanolamine (dansyl-DHPE; Molecular Probes) was included at 5%. The labeled LUVs are designated pLUV and dLUV, respectively. Phospholipid pellets were suspended in buffer with 11 passes in a miniextruder assembly (Avanti Polar Lipids).

Membrane Binding. Membrane binding was monitored by fluorescence resonance energy transfer (FRET) using pyrene-labeled LUVs (pLUV). The spectral overlap between pyrene and heme was used to monitor association of the AOS domain with the membrane. Protein was added to solutions of pLUV (total phospholipid concentration 260 μM) in 50 mM Tris-HCl, pH 7.5, and 500 mM NaCl in a sample volume of 175 μL. Three emission spectra were recorded for each sample in triplicate: (1) protein only, (2) after the addition of $CaCl_2$ to a final concentration of 2 mM, and (3) after the addition of EDTA to a final concentration of 4 mM. The total dilution of the sample after addition of $CaCl_2$ and EDTA was 5%. Protein concentrations in the cuvette were as follows: FP, 2 μM; HD, 2 μM 8*R*-LOX + 3 μM AOS; AOS, 3 μM. All emission spectra were recorded on a Jasco FP-6300 spectrofluorometer with excitation and emission bandwidths set to 2.5 and 5 nm, respectively. The excitation wavelength was set at 280 nm. The spectra (averages of triplicate samples) were not corrected for the 5% dilution.

Ca^{2+}-dependent LOX membrane binding was also monitored in the presence of increasing concentrations of AOS. 8*R*-LOX membrane binding was monitored by FRET using dansyl-labeled liposomes (dLUV) with the assay previously described (*11*). Briefly, the concentration of 8*R*-LOX was held constant at 0.5 μM, and that of AOS ranged from 0.16 to 1.3 μM. Emission spectra (excitation wavelength 295 nm) were recorded for protein in 260 μM dLUV, 50 mM Tris (7.5), and 500 mM NaCl, before and after the addition of 2 mM $CaCl_2$. Measurements were performed in triplicate. Membrane binding was indicated by an increase in dansyl florescence (517 nm). AOS does not exhibit Trp fluorescence due to the presence of heme.

Protein binding to sucrose-loaded vesicles was monitored by ultracentrifugation in a method similar to the one previously described (*29*). LUVs were prepared as described above, but in the presence of 0.2 M sucrose, and diluted 30-fold in 50 mM Tris (pH 7.5) and 150 mM NaCl. 8*R*-LOX or FP was added to a final concentration of 80 nM. AOS was added at 320 nM. The total phospholipid concentration was 80 μM. In these assay conditions the molar ratio of protein to liposomes was ~10:1. The mixture was aliquoted into eight 3 mL volumes to which $CaCl_2$ was added to final concentrations of 0, 16, 31, 63, 125, 250, 500, and 1000 μM. The samples were centrifuged at 100000*g* for 1 h. After ultracentrifugation, the supernatants were immediately decanted, and the pellets were dissolved in SDS loading buffer and applied to a 10% polyacrylamide gel. The intensities of Coomassie-stained bands were integrated with image processing software (Adobe Photoshop, Adobe Systems Inc.).

Susceptibly to Cleavage by TEV-protease. Limited proteolysis experiments were performed to determine the impact of Ca^{2+}-dependent membrane binding on protease site accessibility. AOS-TEVsite-LOX fusion protein (20 μg) was incubated with TEV-protease (Invitrogen) in 50 mM Tris, pH 8, 0.5 mM EDTA, 1 mM DTT, and 260 μM LUV or AA-LUV, in the absence or presence of 2 mM $CaCl_2$. A similar incubation was performed in the presence of the detergent dodecyl maltoside (260 μM) rather than LUV. Samples were maintained at 30 °C for 4 h. The reaction was stopped by the addition of 5× SDS−PAGE sample buffer and boiling. Reaction products were separated by SDS−PAGE in 10% gels. While it has been reported that TEV-protease is inhibited by some detergents, dodecyl maltoside does not affect the protease activity (*30*). The concentrations of phospholipids in the reaction mixtures correspond to those utilized in the FRET membrane binding and standard 8*R*-LOX activity assays. The intensities of Coomassie-stained bands were integrated with image processing software (Adobe Photoshop, Adobe Systems Inc.).

Lipoxygenase Activity of the 8R-Domain. Activity of the 8*R*-LOX domain was measured using a stopped-flow spectrometer (Model SX17MV; Applied Photophysics Ltd.) operating in the absorbance mode at 25 °C (*11, 31*). The Ca^{2+}-stimulated activity of the wild-type 8*R*-LOX domain was monitored in the presence of liposomes composed of either porcine brain PC:PS (3:1) or AA-PC:PS (3:1) as previously described (*11*).

RESULTS

AOS and LOX Form a Complex in the Absence of Covalent Linkage. As mentioned above, and as described in the purification protocol for HD, independently expressed AOS and LOX domains coelute on a sizing column at a volume

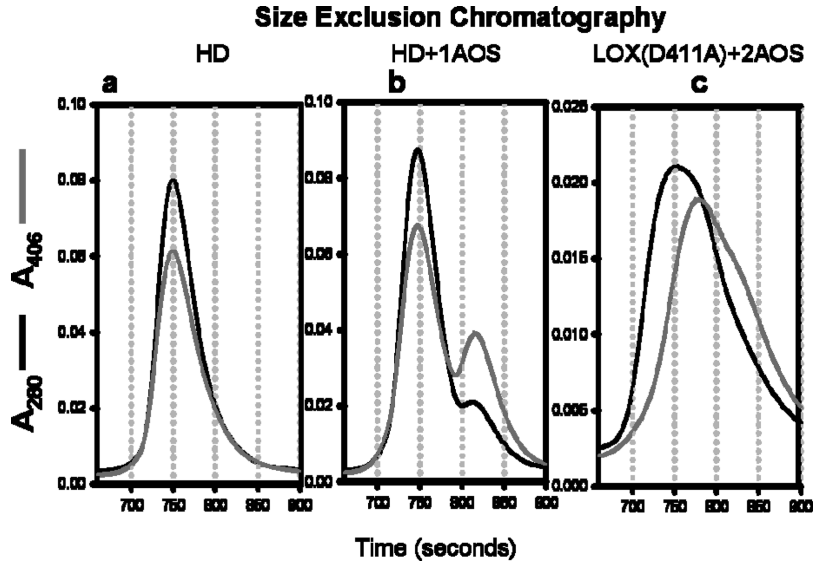

FIGURE 1: Size exclusion chromatography of 8*R*-LOX and AOS. Protein elution was simultaneously monitored at 280 (black) and 406 nm (gray). Absorbance at 406 nm is due to the AOS heme. (a) HD (LOX:AOS) elutes as a complex at 750 s. (b) AOS in excess (2AOS:1LOX) yields two clearly resolved peaks: HD (750 s) and AOS (820 s). HD has 1 heme for 1066 amino acids, and the absorbance at 280 nm is greater than that at 406 nm. The reverse is true for AOS, which has 1 heme for 373 amino acids. (c) A 2:1 mixture of AOS:LOX(D411A). The mutation in the LOX C2-like domain impairs HD formation. Note in panel c the absence of distinct HD and AOS peaks, an indication that a heterodimer of LOX(D411A) + AOS is not stable in the size exclusion chromatography column.

consistent with a molecular mass of 122 kDa: LOX and AOS form an $\alpha\beta$ heterodimer (HD) in the absence of a covalent linkage (Figure 1a). Addition of AOS in excess resulted in two clearly resolved peaks on gel filtration, the earlier eluting AOS-LOX heterodimer and the free AOS at a retention time compatible with its homodimer mass of 86 kDa (Figure 1b). Formation of a complex between the two proteins was disrupted by the D411A mutation in the C2-like domain of 8*R*-LOX (Figure 1c). The peaks are smeared, suggesting that the interactions in D411A-LOX:AOS are weakened and the complex is no longer stable under the gel filtration condition. A similar result was observed for the E419A mutation of 8*R*-LOX (data not shown). (D411 and E419 correspond to D39 and E47, respectively, of the LOX domain in the numbering convention of Oldham et al. (*11*).) D411 and E419 are Ca^{2+}-binding residues located on the C2-like domain proximal to the AOS-LOX covalent linker, and both the D411A and E419A mutants have wild-type activity in a membrane-free assay (*11*). This result and the physical restrictions imposed by the short linker between the two catalytic domains of the natural fusion protein suggest that the C2-like domain mediates noncovalent interactions between AOS and LOX. There are only six amino acids between the last structured residue of the AOS domain and the first structured residue of the LOX domain (*11, 16*), and this short covalent linker is bound to situate AOS close to the C2-like domain of 8*R*-LOX.

The Complex Recapitulates the Structure of the Fusion Protein. SAXS experiments were performed to determine whether HD recapitulates the structure of the native fusion protein. Measurements for both FP and HD were obtained at four concentrations ranging from 1 to 10 mg/mL. The radii of gyration (R_g) values indicate the presence of mild interparticle interference, but the electrostatic properties of the two different protein preparations are indistinguishable (Figure 2a). There is no sign of concentration-dependent aggregation in the concentration range as indicated by nearly constant $I(Q = 0)/c$ values. The ~20% difference in forward scattering intensities of HD and FP is likely due to over/underestimation of the concentrations of the dilute samples prior to concentration by centrifugation. As the R_g values for HD and FP are equivalent, dissociation of HD is not a likely explanation for the difference.

The R_g value extrapolated to zero concentration was 37.5 ± 0.3 Å for both HD and FP. The composite scattering curves for the two preparations, obtained by scaling and merging the scattering curves at 1 and 10 mg/mL, measured at 2.5 and 1.0 m sample-to-detector distance, respectively, are highly similar (Figure 2b). This result indicates that FP and HD have comparable solution structures at the level of tertiary structure. The forward scattered intensities obtained for FP and HD were consistent, within experimental error, with the expected molecular masses as compared with lysozyme scattering intensities that were also recorded using the same experimental setup. If LOX and AOS had been dissociated, a completely different scattering curve would have been observed. The predicted curve for a mixture of LOX monomer and AOS dimer (AOS is a dimer in solution and in the crystal structure) is also shown in Figure 2b.

The pair distance distribution functions for HD and FP are also essentially identical and give a value of 115 Å (~the largest dimension of the LOX domain) for the largest extent of the molecule, further supporting equivalent solution conformations. The SAXS experiments clearly support the supposition that the independently expressed AOS and LOX domains associate to form a heterodimer that recapitulates the structure of the full-length fusion protein. As stable protein−protein interfaces require that complementary surfaces bury ~1000 Å^2 surface area (*32*−*34*), it is highly unlikely that the interface in HD differs from the natural interface in the FP. If the covalent linker were to prevent an *intra*molecular association that is only possible as an *inter*molecular interaction, aggregation or oligomerization of the fusion protein would occur at higher protein concentra-

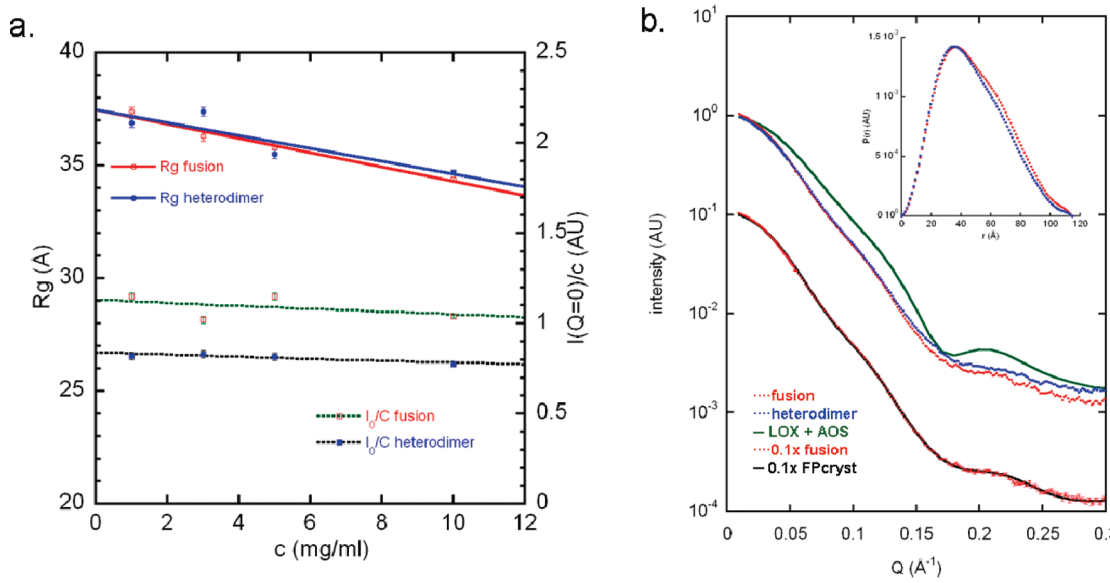

FIGURE 2: Small-angle X-ray scattering of HD and FP. (a) Radii of gyration and the forward scattered intensity divided by protein concentration recorded for FP and HD as a function of concentration. (b) Composite X-ray scattering curves and corresponding electron pair distance distribution function (inset). Those curves for FP are shown in red and HD in blue. Also shown in green is the scattering curve predicted for a mixture of LOX and AOS in 1:2 molar ratio without forming heterodimer, based on corresponding crystallographic structures. The same FP curve (scaled at 0.1×) is reproduced with experimental error bars in the lower part of the figure along with the predicted X-ray scattering curve (black, scaled at 0.1×) for one of the two low-resolution crystal structures of FP.

tions. Yet the fusion protein remains fully soluble at concentrations as high as 26 mg/mL. We also investigated the effects of Ca^{2+} on the FP and HD conformations. In the presence of 2 mM $CaCl_2$, the radii of gyration extrapolated to zero concentration were within 1 Å of the value observed for both HD and FP in the absence of Ca^{2+} (data not shown). This difference in R_g indicates that Ca^{2+} binding does not promote a substantial reorientation of the AOS and LOX domains of FP or impact HD formation.

The Crystal Structure of the Full-Length Fusion Protein. The 3.5 Å resolution structure of the fusion protein includes 365 of 372 residues of the AOS domain and 637 of 694 amino acids of the 8*R*-LOX domain in the asymmetric unit (chains A and C). The putative membrane insertion loops of the C2-like domain were among the parts of the protein not visible in the electron density maps. In addition, despite the inclusion of $CaCl_2$ in the crystallization conditions, electron density cannot be unambiguously attributed to Ca^{2+}. The apparent lack of the cation could be due to the abundance of Ca^{2+} chelators in the crystallization solution but more likely reflects the limited resolution of the crystal structure. The Ca^{2+} binding sites as defined by the structure of the LOX domain (*11*) are accessible, and remnants of electron density are consistent with the binding sites and loops modeled in that work. However, the absence of electron density for amino acids 568−598 is somewhat surprising given that this region is visible in our 3.2 Å LOX structure (*11*). However, this part of the protein is devoid of packing contacts in the FP crystal lattice and is perhaps not sufficiently restrained. In the initial cycles of refinement and map interpretation, there was no electron density for the linker region that joins the AOS and LOX domains (367−372) for either of the two molecules in the asymmetric unit. Moreover, the domains are oriented such that the C-terminus of either AOS module is positioned sufficiently close (10.5 and 13.5 Å) to the amino terminus of a LOX domain to be joined by the covalent linker. Thus the structure of FP could not be determined with the crystallographic data alone. However, the SAXS data are clearly consistent with only one of the two possible conformations of FP in the unit cell and thus allowed us to distinguish which association of domains reflects an *intra*molecular interaction (Figure 2b). After the R_{work}/R_{free} reached 27.3/32.2, electron density was visible for a linker between the AOS and LOX domains of one of the monomers (chain C) in the asymmetric unit (the termini separated by 13.5 Å). Furthermore, the linkage is exactly what was predicted by the SAXS-supported model illustrated in Figure 3. Accordingly, the SAXS data support our interpretation of this density as the linker and indicate that the orientation of the catalytic domains in the crystal lattice reflects the solution structure of FP.

Note that in the FP structure (Figure 3) helix α2 of AOS makes contacts with both the C2-like and catalytic subdomains of LOX. The intramolecular interface buries ∼1000 Å^2 surface area of each component (*35*) and is dominated by polar and charged interactions. Approximately 40% of the LOX interface is provided by the C2-like domain, and this interaction does not involve the membrane insertion loops or the Ca^{2+} binding amino acids (e.g., D419). Consistent with our observation that the addition of Ca^{2+} does not induce a conformational change detectable in SAXS experiments, AOS does not obstruct access to the Ca^{2+}-binding amino acids.

The independently expressed AOS domain is a dimer with an interface formed by a parallel interaction of helices α2 from each of the monomers (*16*). Therefore, its participation on the AOS-8*R*-LOX interface is consistent with the fact that we have never observed dimerization of FP or association of free AOS with FP or HD, assemblies which would require that helix α2 is free to make the contacts it does in the AOS dimer. In the FP structure, helix α2 is flanked by the C-terminal helix of the AOS domain and the C-terminal helix of the LOX domain (Figure 3b).

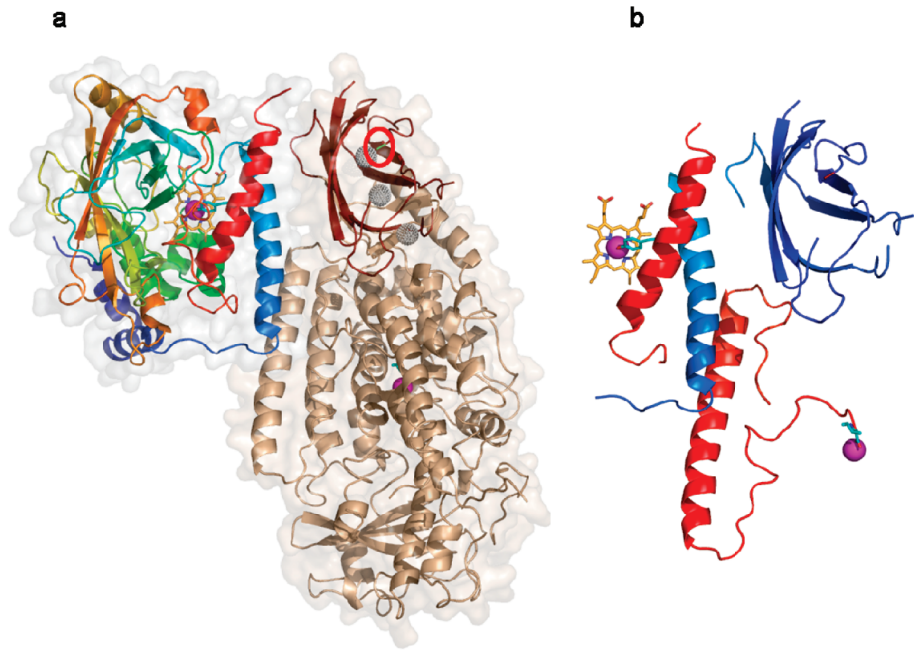

FIGURE 3: SAXS-supported crystal structure of FP. (a) A cartoon and surface rendering of FP. The AOS domain is colored N → C (blue → red). The C2-like and catalytic subdomains of the LOX portion are in brown and beige, respectively. The gray spheres mark the positions of the Ca^{2+} atoms in the 3.2 Å resolution structure of the LOX domain alone (2FNQ). Neither the Ca^{2+} ions or the putative membrane insertion loops that they stabilize (one of which includes D411, position marked by red oval) are observed with confidence in the FP structure. (b) Detail of the structural elements that make up the AOS-LOX interface. In this rendering, which is identical in orientation as in (a), the LOX domain is also colored N → C (blue → red). Amino-terminal AOS helix α2 (blue) is flanked by C-terminal helices of both the AOS and LOX domains (red). Amino acid ligands for the catalytic irons of both domains are directly (AOS) or indirectly (LOX) connected to these helical segments.

The Fusion Protein Binds Membrane in a Ca^{2+}-Dependent Manner. It was previously reported that the independently expressed 8*R*-LOX domain binds membrane in a Ca^{2+}-dependent manner and that the C2-like domain amino acids D411 and E419 are required for membrane binding but not enzymatic activity (*11*). In addition, a deletion mutant that lacks a putative membrane insertion loop in the C2-like domain does not display Ca^{2+}-stimulated activity in a membrane-based assay but has wild-type activity in the absence of membranes. Furthermore, in conditions in which the wild-type enzyme is found in the membrane fraction, the LOX deletion mutant is soluble (*15*). In an effort to determine how the presence of AOS might impact the membrane binding function of the 8*R*-LOX C2-like domain, we monitored Ca^{2+}-dependent membrane targeting of FP, 8*R*-LOX, and HD by FRET and ultracentrifugation assays.

FRET data suggest that despite the fact that AOS and LOX form a noncovalent complex, AOS is not localized to the membrane unless covalently bound to 8*R*-LOX. AOS membrane binding was monitored with LUVs prepared with the fluorophore pryene incorporated into the phospholipid headgroup (pLUV). The overlap of the pyrene fluorescence and heme absorbance spectra is such that FRET between the pyrene−heme donor−acceptor pair occurs when they are proximal. Each spectrum presented in Figure 4a represents the average of three independent measurements. Upon the addition of $CaCl_2$ to a final concentration of 2 mM to FP in the presence of pLUV, a 16% loss of pyrene fluorescence at 381 nm was observed, consistent with a membrane-proximal location for heme (Figure 4a). This signal is 9σ, where σ is the standard deviation of the triplicate measurements. Addition of EDTA in excess restored the pyrene fluorescence to 95% of its original value, a value indicative of total recovery of signal if the 5% dilution of sample that occurs with the addition of $CaCl_2$ and EDTA is taken into consideration. Equivalent experiments were performed with LOX in the presence of an excess of AOS (1.5 equiv) and with AOS alone. No differences above 1σ were observed for the spectra in the three conditions for either HD or AOS alone; i.e., spectra obtained after the addition of Ca^{2+} and EDTA were within the standard deviation of triplicate measurements of the initial conditions. Thus, heme is not brought into proximity of the membrane by the addition of Ca^{2+} when AOS is not covalently bound to LOX.

Since the AOS domain does not colocalize to the membrane with LOX unless it is covalently linked as it is in the fusion protein and the C2-like domain that mediates membrane binding is positioned between the LOX catalytic domain and the AOS domain, we asked whether membrane and AOS binding by LOX are mutually exclusive. We utilized the Trp to dansyl-labeled LUV FRET assay previously described (*11*) to determine whether AOS inhibits Ca^{2+}-dependent membrane binding by 8*R*-LOX. We observed that, in the presence of increasing amounts of AOS in the FRET assay, fluorescence at 517 nm decreased, consistent with inhibition of membrane binding of 8*R*-LOX by AOS (Figure 4b). AOS is a heme protein, and thus the intrinsic Trp fluorescence of AOS is fully quenched. An alternate interpretation of the AOS titration data is simply that there is physical interaction of AOS with 8*R*-LOX, and this proximity quenches the signal of the Trp residues of the LOX C2-like domain and as a consequence resonance energy transfer to the dansyl fluorophore. However, we are able to rule out this interpretation with the pyrene−heme FRET data, and the ultracentrifugation data described below, that clearly indicate that AOS is not localized to the

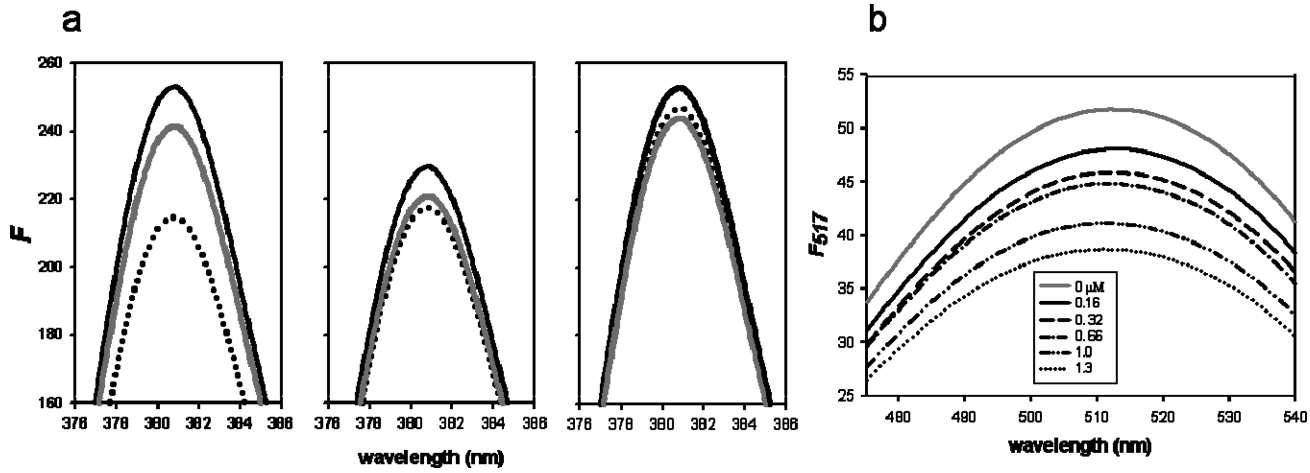

FIGURE 4: Membrane binding monitored by FRET. (a) Pyrene−heme FRET. Emission spectra for pyrene-labeled liposomes and fusion protein (FP, left), heterodimer (HD, middle), and AOS (right). Protein was added to solutions of LUV in which pyrene-labeled phospholipid was incorporated. Emission spectra were recorded for triplicate samples in three states: protein only (solid black), plus $CaCl_2$ to a final concentration of 2 mM (dashed line), and plus EDTA to a final concentration of 4 mM (solid gray). For FP, the addition of $CaCl_2$ quenches the observed fluorescence, and the subsequent addition of EDTA restores the signal (the spectra are not corrected for dilution). In contrast, no difference is observed for either the HD or AOS samples in the three states. Thus heme, the prosthetic group of AOS, is only localized to the membrane by Ca^{2+} when covalently bound to LOX. (b) AOS titration of Ca^{2+}-dependent membrane binding by 8*R*-LOX. Emission spectra for 8*R*-LOX alone (0.5 μM, solid black) and in the presence of increasing AOS (from 0.16 to 1.3 μM). Ca^{2+}-dependent binding of 8*R*-LOX to LUV can be measured by FRET when dansyl-labeled phospholipids are incorporated into the vesicles (dLUV (*11*)). Titration of the sample with AOS results in a quench of the dansyl signal.

membrane unless covalently bound to 8*R*-LOX. Loss of F517 with increasing AOS, therefore, is likely indicative of overlap *or* communication between the AOS and membrane binding sites of the 8*R*-LOX C2-like domain. LOX binds either AOS or membranes, but not simultaneously.

Results of additional membrane binding assays support the interpretation that AOS does not accompany LOX to the membrane in the absence of a covalent linkage and that the presence of AOS impacts LOX membrane affinity. In these experiments, membrane targeting of FP, 8*R*-LOX, and HD to sucrose-loaded LUVs was monitored by ultracentrifugation in the presence of 0−1 mM Ca^{2+} followed by SDS−PAGE of the LUV−protein pellets and Coomassie blue staining. Figure 5a shows the total amount of FP, 8*R*-LOX, or HD protein used in each test run. The next panel (Figure 5b) shows the amount of these proteins recovered in the 100000*g* pellet after incubation with LUVs at different Ca^{2+} concentrations. The top panel of bands in Figure 5b (LOX-only incubations) shows that, in the absence of calcium, no LOX protein was pelleted, while the lowest [Ca^{2+}] tested (16 μM) induced translocation, and the amount of protein in the membrane fraction increased with higher Ca^{2+} concentrations. The middle panel of Figure 5b shows the Ca^{2+} dependence of translocation of the fusion protein. As commented on below, the total amount of fusion protein (FP) translocated was less than for LOX alone. The lower panel (HD) shows that calcium-induced translocation of LOX takes place, but not that of AOS, in the absence of a covalent linker.

The intensities of the protein bands in Figure 5b were quantified by densitometric scanning, and the results are summarized in Figure 5c. This analysis clearly shows that membrane binding by LOX alone, as a fusion protein, or as a heterodimer, is calcium-dependent. Furthermore, translocation of AOS to the membrane requires a covalent linker to LOX. An additional point that emerges from this analysis is that the presence of AOS, whether covalently bound or

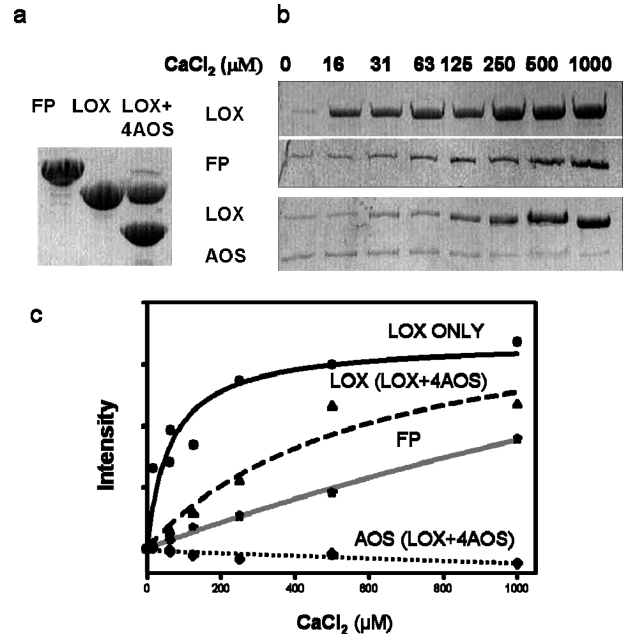

FIGURE 5: Protein pelleting with sucrose-loaded LUVs. (a) An amount equivalent to the total protein in the incubation mixture applied to an SDS−PAGE gel. (b) Protein pelleted with sucrose-loaded LUV as a function of Ca^{2+} concentration. Protein and sucrose-loaded LUV, at concentrations of $CaCl_2$ from 0 to 1 mM, were centrifuged at 100000*g* for 1 h. Membrane fractions were applied to a 10% SDS−PAGE, and the protein was visualized by Coomassie staining. (c) A plot of the intensity of the protein bands vs $CaCl_2$ concentration. Free AOS (dotted line) does not translocate to the membrane in the presence of its partner protein LOX.

not (FP, HD), attenuates the Ca^{2+}-dependent targeting of 8*R*-LOX. The most likely explanation for this effect is that the C2-like domain of 8*R*-LOX is involved in the interactions with AOS and with the membrane, and there is competition between these dual functions. Thus the membrane targeting function of the C2-like domain is functional in the fusion

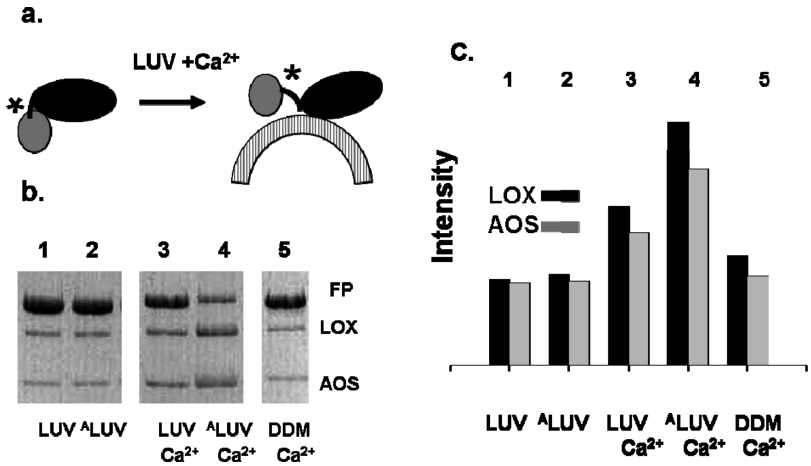

FIGURE 6: Accessibility to the TEV-protease cleavage site. (a) Cartoon of the model for membrane binding by the FP. The TEV-protease site is positioned in the linker between the AOS and LOX domains (indicated by ∗). Ca^{2+}-dependent membrane binding releases AOS from the noncovalent interactions and results in improved access to the TEV cleavage site by protease. (b) TEV-FP was incubated with TEV-protease in buffer plus LUV prepared from 3:1 PC:PS (LUV) or 3:1 AA-PC:PS (^{A}LUV) in the presence or absence of 2 mM $CaCl_2$. A parallel incubation was performed with dodecyl maltoside (300 μM) in place of LUV. The reaction was stopped after 4 h, and the products were separated by SDS−PAGE and visualized with Coomassie stain. (c) A plot of the integrated LOX and AOS band intensities for the gel in (b). Baseline levels of LOX and AOS are observed in the presence of LUV but in the absence of Ca^{2+} (lanes 1 and 2) or in the presence of Ca^{2+} and detergent (lane 5). The addition of Ca^{2+}, which promotes membrane binding of TEV-FP, results in an increase in the LOX and AOS produced. When the liposomes contain AA-PL, the stimulation is enhanced. Thus the phospholipid content impacts TEV-protease susceptibility only in the presence of Ca^{2+}, conditions which promote membrane binding of FP.

protein, but the presence of AOS significantly attenuates membrane affinity in the conditions of the assay.

Membrane Binding Induces a Conformational Change in the Fusion Protein. The C2-like domain of 8*R*-LOX mediates LOX−membrane interaction (*11*) or LOX−AOS interaction (Figure 1), but not both simultaneously (Figures 4 and 5). These data are consistent with either overlap of the membrane and AOS binding sites or some means of communication between distinct binding sites. While the crystal structure, combined with the SAXS data, eliminates the site-overlap interpretation, the limited resolution of the X-ray crystallographic data makes it impossible to infer a mechanism for communication between the membrane-binding and AOS interaction sites. Nonetheless, the data described above combine to suggest that membrane binding by FP induces a conformational change which releases AOS from its noncovalent interaction with LOX and frees up the C2-like domain for interaction with the bilayer. In an effort to detect such a conformational change, we engineered a mutant form of FP that contains a site for TEV-protease cleavage between AOS and LOX. The engineered FP, designated TEV-FP, has wild-type enzymatic and membrane binding activities and is indistinguishable from the wild-type protein in SAXS measurements (data not shown).

The engineered FP that harbors the TEV-protease site has an additional six residues in the linker region. Because the linker is still relatively short, access to the recognition site by TEV-protease is hindered by the AOS and LOX domains. An intramolecular association of the AOS and LOX domains would further restrict access to the cleavage site. The results of the TEV-protease susceptibility assay (Figure 6), performed in quintuplicate, suggest that access to the TEV cleavage site of TEV-FP is enhanced in the presence of Ca^{2+} and membranes. The yields of free LOX and AOS were reproducibly increased when 2 mM $CaCl_2$ was added to the liposome TEV-FP incubation, conditions which promote membrane binding by FP. In addition, a concomitant decrease in the amount of TEV-FP was observed. The integrated intensities of the LOX and AOS bands are depicted in Figure 6b. Note that in the absence of calcium (lanes 1 and 2) or membranes (lane 5) the amount of cleavage of FP is low, and similar amounts of LOX and AOS are produced. (The sum of the intensities of the AOS and LOX bands in lanes 1, 2, and 5 (unstimulated cleavage) varies by less than 10%, and the FP band intensities vary by 12%.) If both membranes and calcium were present (lanes 3 and 4), the sums of the AOS and LOX bands are ∼2 and ∼3 times greater than those in lanes 1, 2, or 5. TEV-protease assays performed in the presence of $CaCl_2$ (but absence of membranes) do not yield significant increases in the amounts of free LOX and AOS (data not shown) produced. This observation is consistent with the fact that we are unable to detect a Ca^{2+} -induced change in the R_g of the fusion protein by SAXS.

No Ca^{2+}-dependent stimulation of proteolysis of FP was observed in the presence of 300 μM dodecyl maltoside (lane 5); hence increased susceptibility to proteolysis depends on the presence of both Ca^{2+} and membranes. In contrast, more AOS and LOX are generated from FP in the presence of arachidonylphospholipids (compare lanes 3 and 4). More significantly, the impact of AA-LUV on TEV-site accessibility parallels the increase in LOX activity observed in the presence of arachidonyl-PC-containing liposomes relative to that observed with porcine brain PC-containing vesicles. The enzymatic activity of 8*R*-LOX was 3-fold higher when AA-PC was substituted for porcine brain PC in 3:1 PC:PS liposomes (data not shown). 8*R*-LOX activity with PC-esterified AA is not measurable in these assay conditions. Consequently, the increased LOX activity with AA-LUV is likely due to enhanced LUV binding by 8R-LOX and indicative of interaction of 8*R*-LOX with liposomes.

DISCUSSION

Although AOS and 8*R*-LOX naturally occur as a fusion protein, we have demonstrated that the two protein domains associate in the absence of a covalent linker. Small-angle X-ray scattering data suggest that the solution structures of the reconstituted heterodimer and full-length fusion protein are indistinguishable. The SAXS data are also consistent with a model of FP inferred from a low-resolution X-ray diffraction data. Despite the noncovalent association of the LOX and AOS domains, AOS shows Ca^{2+}-dependent membrane binding only when it is covalently linked to LOX. These results indicate that the LOX−membrane interaction is not compatible with LOX−AOS domain interaction. Furthermore, SEC data and membrane binding experiments indicate that both interactions require intact Ca^{2+} sites in the C2-like domain. In contrast, the LOX−AOS interface revealed by a SAXS-supported crystal structure of FP does not include the Ca^{2+} binding amino acids or putative membrane insertion loops of the C2-like domain. However, the proximity of these membrane-binding structural elements to the AOS domain in FP is indeed consistent with a model in which membrane binding by the LOX C2-like domain destabilizes the noncovalent AOS and LOX domain interactions, given that the membrane insertion loops of the C2-like domains must penetrate the bulky membrane bilayer. What is less easily reconciled with the model is the observation that the point mutation D411A also disrupts this domain interaction, as D411 and the membrane loop that it stabilizes are outside the AOS and LOX domain interaction surface. However, the absence of a negative charge at this position in the C2-like domain could have structural consequences that affect the AOS−LOX interface.

Membrane binding by LOX *in vitro* is attenuated when it is covalently linked to AOS, as higher $CaCl_2$ concentrations are required to target FP to the membrane than 8*R*-LOX alone (Figure 5). Additionally, when free AOS is included in the membrane binding assay of the free 8R-LOX domain, higher Ca^{2+} concentrations are required for translocation of LOX to the membrane. *In vivo* the lower affinity of FP for membranes may be mitigated by a higher membrane to protein ratio or by the advantage of having the AOS and LOX activities proximal for transfer of the reactive hydroperoxide intermediate. Alternatively, the attenuation might be relieved by some yet unidentified protein partner or signal.

Membrane binding induces a conformational change in FP. Insertion of a highly specific protease cleavage site into a structurally defined position that links two independently folded globular domains allowed us to monitor the intramolecular association of the domains in FP under a variety of conditions. Limited proteolysis is routinely used to reveal conformational changes induced by ligand binding in both single domain (*36, 37*) and multidomain (*38, 39*) proteins, and limited proteolysis has also been used to remove the C2-like domain in soybean LOX-1 and generate a mini-lipoxygenase with only a catalytic domain (*40, 41*). In this work, the engineered TEV-FP allowed us to specifically probe access to the linker region that joins AOS and LOX.

The SAXS-supported crystal structure of FP is depicted in Figure 3. The carboxyl terminus of AOS (red) is joined to the amino terminus of LOX by a linker region not visible in the original electron density maps. The LOX domain is comprised of two subdomains: the C2-like domain that mediates Ca^{2+}-dependent membrane binding (*11, 15*) and the catalytic domain. Our data indicate that the Ca^{2+}-dependent membrane binding activity is functional in the naturally occurring fusion protein and that, as a consequence, the covalent linker that joins the AOS and LOX domains provides a means to colocalize the downstream enzyme activity at the membrane, perhaps facilitating transfer of the reaction intermediate between sequential catalytic activities. Significantly, incubation of FP with phospholipid vesicles that incorporate AA-PC increased TEV-protease susceptibility relative to that observed with LUV prepared with standard porcine brain phospholipids. This enhanced protease susceptibility correlates with an increased enzyme activity of the LOX domain. When LOX was assayed in the presence of liposomes, Ca^{2+}-stimulated enzyme activity in the presence of 3:1 AA-PC:PS was 3-fold greater than that measured in the presence of 3:1 porcine brain PC:PS.

The calcium binding residues of the 8*R*-lipoxygenase domain and putative membrane insertion residues are also present in human 5-LOX, the enzyme that initiates the leukotriene biosynthetic pathway. Ca^{2+} targets 5-LOX to the nuclear membrane (*42*−*44*), which is rich in arachidonylphospholipids. Furthermore, the C2-like domain of 5-LOX mediates Ca^{2+}-dependent targeting (*14, 45, 46*). While Ca^{2+}-dependent membrane binding activity has been localized to the C2-like domain for 5- and 8*R*-lipoxygenases, this is not the case for 15-LOX. The association of 15-LOX with the membrane requires surface-exposed hydrophobic amino acids in both the C2-like and catalytic domains (*47*). This observation is consistent with key sequence differences among LOX isozymes. While Ca^{2+} binding amino acids and putative membrane insertion loops are conserved in 5- and 8*R*-lipoxygenases, as well as the C2-like domain of the α-toxin phospholipase (*46, 48*), these features are absent in 15-LOX and other LOX isozymes.

Pande et al. demonstrated that membrane fluidity modulates membrane binding by 5-LOX. In addition, membrane penetration by the enzyme (as determined by Trp insertion into the bilayer) and enzyme activity are enhanced with phospholipid cis desaturation (*49, 50*). Our results suggest that membrane desaturation impacts the ability of the 8*R*-lipoxygenase domain to penetrate the bilayer, since liposomes that contain AA as an esterified fatty acid promote TEV-protease cleavage of TEV-FP, consistent with a membrane-induced conformational change.

Arachidonic acid serves as a precursor to numerous biologically active compounds, including the prostaglandins, leukotrienes, and thromboxanes, collectively known as eicosanoids. Biosynthesis of prostaglandins and thromboxanes proceeds *via* the cyclooxygenase pathway in which prostaglandin H synthase (also known as cyclooxygenase, COX) converts arachidonic acid in two enzymatic steps to prostaglandin H2 (*51*). The leukotrienes are derived from the lipoxygenase (LOX) pathway, in which 5-LOX catalyzes the two-step conversion of AA to leukotriene A4 (*52*). Eicosanoids are known as local hormones, since they exert their effects on cells close to their sites of synthesis and are rapidly degraded. Like the products of these biosynthetic pathways, the intermediates are both labile and of limited solubility. One way to optimize acquisition of a hydrophobic or labile substrate is to associate enzymes of the metabolic

pathways either covalently or noncovalently. Mandel et al. (*53*) suggested that discrete protein complexes determine the fates of leukotriene intermediates (e.g., the relative amounts of leukotrienes C4 vs B4 produced). Similarly, prostaglandin biosynthetic pathways have branch points that must be navigated by the intermediates common to multiple prostaglandin products that induce fundamentally different, and often opposing, biological responses. In an effort to determine whether colocalization of enzymatic activities might impact the relative amounts of prostacyclin (PGI2) and thromboxane A2 produced, a bifunctional enzyme that contained both cyclooxygenase (required for the biosynthesis of both products) and PGI2 synthase was engineered (*54*). Indeed, cells expressing this construct produced elevated levels of PGI2 (*54*). In addition, Farmaki et al. (*55*) have reported the colocalization of lipoxygenase, allene oxide synthase, and allene oxide cyclase, sequential catalytic activities in the biosynthesis of jasmonic acid in plants. These results suggest that the segregation of enzymes can regulate metabolic flux through alternative branches of biosynthetic pathways. Macromolecular assemblies are likely a common theme in lipid−mediator biosynthesis in plants and animals, and the naturally occurring fusion of the allene oxide synthase to a Ca^{2+}-dependent LOX is an example of how the covalent linkage of sequential activities confers Ca^{2+}-dependent membrane binding on an otherwise soluble partner protein.

In the coral AOS-LOX fusion protein, the AOS and LOX catalytic domains flank a Ca^{2+}-dependent membrane targeting module, and AOS binding is not compatible with membrane binding by the C2-like domain. A similar competition between protein−membrane-lipid and protein−protein interactions has been described for protein kinase Cα and RhoGTPases. In this case the C2 domain of protein kinase Cα mediates membrane binding and RhoGTPase interaction in an either/or fashion (*56*). As a consequence of the covalent fusion of AOS and LOX, Ca^{2+}-dependent membrane binding by the LOX C2-like domain results in membrane localization of both enzymatic activities. An additional advantage of joining the AOS and LOX activities in a single polypeptide is suggested in Figure 3b. Note that helix α2 is flanked by the C-terminal helices of both the AOS and LOX domains. The AOS C-terminal helix provides the proximal Tyr heme ligand for the active site prosthetic group. In LOX, the C-terminal helix is followed by a 17 amino acid loop that penetrates the helical bundle of the catalytic domain so that the carboxylate of the C-terminal Ile fills the coordination sphere of the active site iron. One might speculate that this arrangement, in which a single helix could impact the conformations of active site ligands for both domains, allows for communication between the two catalytic sites.

REFERENCES

1. Soberman, R. J., and Christmas, P. (2003) The organization and consequences of eicosanoid signaling. *J. Clin. Invest. 111*, 1107–1113.
2. Peters-Golden, M., and Brock, T. G. (2000) Intracellular compartmentalization of leukotriene biosynthesis. *Am. J. Respir. Crit. Care Med. 161*, S36–S40.
3. Peters-Golden, M., and Brock, T. G. (2001) Intracellular compartmentalization of leukotriene synthesis: unexpected nuclear secrets. *FEBS Lett. 487*, 323–326.
4. Brash, A. R. (1999) Lipoxygenases: occurrence, functions, catalysis, and acquisition of substrate. *J. Biol. Chem. 274*, 23679–23682.
5. Kuhn, H., and Thiele, B. J. (1999) The diversity of the lipoxygenase family. Many sequence data but little information on biological significance. *FEBS Lett. 449*, 7–11.
6. Kuhn, H., Saam, J., Eibach, S., Holzhutter, H. G., Ivanov, I., and Walther, M. (2005) Structural biology of mammalian lipoxygenases: enzymatic consequences of targeted alterations of the protein structure. *Biochem. Biophys. Res. Commun. 338*, 93–101.
7. Boyington, J. C., Gaffney, B. J., and Amzel, L. M. (1990) Crystallization and preliminary X-ray analysis of soybean lipoxygenase-1, a non-heme iron-containing dioxygenase. *J. Biol. Chem. 265*, 12771–12773.
8. Minor, W., Steczko, J., Stec, B., Otwinowski, Z., Bolin, J. T., Walter, R., and Axelrod, B. (1996) Crystal structure of soybean lipoxygenase L-1 at 1.4 Å resolution. *Biochemistry 35*, 10687–10701.
9. Skrzypczak-Jankun, E., Amzel, L. M., Kroa, B. A., and Funk, M. O. (1997) Structure of soybean lipoxygenase L3 and a comparison with its L1 isoenzyme. *Proteins: Struct., Function., Genet. 29*, 15–31.
10. Gillmor, S. A., Villasenor, A., Fletterick, R., Sigal, E., and Browner, M. F. (1997) The structure of mammalian 15-lipoxygenase reveals similarity to the lipases and the determinants of substrate specificity. *Nat. Struct. Biol. 4*, 1003–1009.
11. Oldham, M. L., Brash, A. R., and Newcomer, M. E. (2005) Insights from the X-ray crystal structure of coral 8R-lipoxygenase: calcium activation via A C2-like domain and a structural basis of product chirality. *J. Biol. Chem. 280*, 39545–39552.
12. Youn, B., Sellhorn, G. E., Mirchel, R. J., Gaffney, B. J., Grimes, H. D., and Kang, C. (2006) Crystal structures of vegetative soybean lipoxygenase VLX-B and VLX-D, and comparisons with seed isoforms LOX-1 and LOX-3. *Proteins 65*, 1008–1020.
13. Rizo, J., and Sudhof, T. C. (1998) C2-domains, structure and function of a universal Ca^{2+}-binding domain. *J. Biol. Chem. 273*, 15879–15882.
14. Cho, W., and Stahelin, R. V. (2006) Membrane binding and subcellular targeting of C2 domains. *Biochim. Biophys. Acta 1761*, 838–849.
15. Neau, D. B., Gilbert, N. C., Bartlett, S. G., Dassey, A., and Newcomer, M. E. (2007) Improving protein crystal quality by selective removal of a Ca^{2+}-dependent membrane-insertion loop. *Acta Crystallogr., Sect. F 63*, 972–975.
16. Oldham, M. L., Brash, A. R., and Newcomer, M. E. (2005) The structure of coral allene oxide synthase reveals a catalase adapted for metabolism of a fatty acid hydroperoxide. *Proc. Natl. Acad. Sci. U.S.A. 102*, 297–302.
17. Corey, E., Washburn, W., and Chen, J. (1972) Studies on prostaglandin A2 synthetase complex from *Plexaura homomalla*. *J. Am. Chem. Soc. 95*, 2054–2055.
18. Koljak, R., Boutaud, O., Shieh, B. H., Samel, N., and Brash, A. R. (1997) Identification of a naturally occurring peroxidase-lipoxygenase fusion protein. *Science 277*, 1994–1996.
19. Tijet, N., and Brash, A. R. (2002) Allene oxide synthases and allene oxides. *Prostaglandins Other Lipid Mediat. 68−69*, 423–431.
20. Corey, E. J., Matsuda, S. P. T., Nagata, R., and Cleaver, M. B. (1988) Biosynthesis of 8-R-HPETE and preclavulone-A from arachidonate in several species of caribbean coral. A wide-spread route to marine prostanoids. *Tetrahedron Lett. 29*, 2555–2558.
21. Corey, E. J., d'Alarcao, M., Matsuda, S. P. T., Lansbury, P. T., and Yamada, Y. (1987) Intermediacy of 8-(R)-HPETE in the conversion of arachidonic-acid to pre-clavulone-a by *clavularia-viridis*—implications for the biosynthesis of marine prostanoids. *J. Am. Chem. Soc. 109*, 289–290.
22. Marcotte, E. M., Pellegrini, M, Ng, H.-L., Rice, D. W., Yeates, T., and Eisenberg, D. (1999) Detecting protein function and protein-protein interactions from genome sequences. *Science 285*, 751–753.
23. Smolsky, I. L., Liu, P., Niebuhr, M., Ito, K., Weiss, T. M., and Tsuruta, H. (2007) Biological small-angle X-ray scattering facility at the Stanford synchrotron radiation laboratory. *J. Appl. Crystallogr. 40*, S453−S458.
24. Konarev, P. V., Volkov, V. V., Sokolova, A. V., Koch, M. H. J., and Svergun, D. I. (2003) PRIMUS: a Windows PC-based system for small-angle scattering data analysis. *J. Appl. Crystallogr. 36*, 1277–1282.
25. Svergun, D. I., Semenyuk, A. V., and Feigin, L. A. (1988) Small-angle-scattering-data treatment by the regularization method. *Acta Crystallogr., Sect. A 44*, 244–250.

26. Svergun, D., Barberato, C., and Koch, M. H. J. (1995) CRYSOL—a program to evaluate X-ray solution scattering of biological macromolecules from atomic coordinates. *J. Appl. Crystallogr. 28*, 768–773.
27. Otwinowski, Z., Minor, W., and Carter, C. W. (1997) Processing of X-ray diffraction data collected in oscillation mode. *Methods Enzymol.,* 307–326.
28. Collaborative Computational Project, No. 4. (1994) The CCP4 suite: programs for protein crystallography. *Acta Crystallogr., Sect. D: Biol. Crystallogr. 50*, 760–763.
29. Jenco, J. M., Becker, K. P., and Morris, A. J. (1997) Membrane-binding properties of phospholipase C-beta1 and phospholipaseC-beta2: role of the C-terminus and effects of polyphosphoinositides, G-proteins and Ca^{2+}. *Biochem. J. 327*, 431–437.
30. Mohanty, A. K., Simmons, C. R., and Wiener, M. C. (2003) Inhibition of tobacco etch virus protease activity by detergents. *Protein Expression Purif. 27*, 109–114.
31. Boutaud, O., and Brash, A. R. (1999) Purification and catalytic activities of the two domains of the allene oxide synthase-lipoxygenase fusion protein of the coral *Plexaura homomalla*. *J. Biol. Chem. 274*, 33764–33770.
32. Janin, J., and Chothia, C. (1990) The structure of protein-protein recognition sites. *J. Biol. Chem. 265*, 16027–16030.
33. Nooren, I. M., and Thornton, J. M. (2003) Diversity of protein-protein interactions. *EMBO J. 22*, 3486–3492.
34. Nooren, I. M., and Thornton, J. M. (2003) Structural characterisation and functional significance of transient protein-protein interactions. *J. Mol. Biol. 325*, 991–1018.
35. Krissinel, E., and Henrick, K. (2007) Inference of macromolecular assemblies from crystalline state. *J. Mol. Biol. 372*, 774–797.
36. Jamison, R. S., Newcomer, M. E., and Ong, D. E. (1998) Detection of conformational changes in cellular retinoid-binding proteins by limited proteolysis. *Methods Mol. Biol. 89*, 165–176.
37. Davletov, B. A., and Sudhof, T. C. (1994) $Ca^{(2+)}$-dependent conformational change in synaptotagmin I. *J. Biol. Chem. 269*, 28547–28550.
38. Che, M. M., Boja, E. S., Yoon, H. Y., Gruschus, J., Jaffe, H., Stauffer, S., Schuck, P., Fales, H. M., and Randazzo, P. A. (2005) Regulation of ASAP1 by phospholipids is dependent on the interface between the PH and Arf GAP domains. *Cell Signalling 17*, 1276–1288.
39. Dokudovskaya, S., Williams, R., Devos, D., Sali, A., Chait, B. T., and Rout, M. P. (2006) Protease accessibility laddering: a proteomic tool for probing protein structure. *Structure 14*, 653–660.
40. Di Venere, A., Salucci, M. L., van Zadelhoff, G., Veldink, G., Mei, G., Rosato, N., Finazzi-Agro, A., and Maccarrone, M. (2003) Structure-to-function relationship of mini-lipoxygenase, a 60-kDa fragment of soybean lipoxygenase-1 with lower stability but higher enzymatic activity. *J. Biol. Chem. 278*, 18281–18288.
41. Maccarrone, M., Salucci, M. L., van Zadelhoff, G., Malatesta, F., Veldink, G., Vliegenthart, J. F., and Finazzi-Agro, A. (2001) Tryptic digestion of soybean lipoxygenase-1 generates a 60 kDa fragment with improved activity and membrane binding ability. *Biochemistry 40*, 6819–6827.
42. Rouzer, C. A., and Kargman, S. (1988) Translocation of 5-lipoxygenase to the membrane in human leukocytes challenged with ionophore A23187. *J. Biol. Chem. 263*, 10980–10988.
43. Wong, A., Cook, M. N., Foley, J. J., Sarau, H. M., Marshall, P., and Hwang, S. M. (1991) Influx of extracellular calcium is required for the membrane translocation of 5-lipoxygenase and leukotriene synthesis. *Biochemistry 30*, 9346–9354.
44. Brock, T. G., and Healy, A. M. (2000) Nuclear import of arachidonate 5-lipoxygenase. *Arch. Immunol. Ther. Exp. 48*, 481–486.
45. Chen, X. S., and Funk, C. D. (2001) The N-terminal "beta-barrel" domain of 5-lipoxygenase is essential for nuclear membrane translocation. *J. Biol. Chem. 276*, 811–818.
46. Kulkarni, S., Das, S., Funk, C. D., Murray, D., and Cho, W. (2002) Molecular basis of the specific subcellular localization of the C2-like domain of 5-lipoxygenase. *J. Biol. Chem. 277*, 13167–13174.
47. Walther, M., Wiesner, R., and Kuhn, H. (2004) Investigations into calcium-dependent membrane association of 15-lipoxygenase-1. Mechanistic roles of surface-exposed hydrophobic amino acids and calcium. *J. Biol. Chem. 279*, 3717–3725.
48. Naylor, C. E., Jepson, M., Crane, D. T., Titball, R. W., Miller, J., Basak, A. K., and Bolgiano, B. (1999) Characterisation of the calcium-binding C-terminal domain of *Clostridium perfringens* alpha-toxin. *J. Mol. Biol. 294*, 757–770.
49. Pande, A. H., Moe, D., Nemec, K. N., Qin, S., Tan, S., and Tatulian, S. A. (2004) Modulation of human 5-lipoxygenase activity by membrane lipids. *Biochemistry 43*, 14653–14666.
50. Pande, A. H., Qin, S., and Tatulian, S. A. (2005) Membrane fluidity is a key modulator of membrane binding, insertion, and activity of 5-lipoxygenase. *Biophys. J. 88*, 4084–4094.
51. Rouzer, C. A., and Marnett, L. J. (2003) Mechanism of free radical oxygenation of polyunsaturated fatty acids by cyclooxygenases. *Chem. Rev. 103*, 2239–2304.
52. Radmark, O. (2002) Arachidonate 5-lipoxygenase. *Prostaglandins Other Lipid Mediat. 68−69*, 211–234.
53. Mandal, A. K., Skoch, J., Bacskai, B. J., Hyman, B. T., Christmas, P., Miller, D., Yamin, T. T., Xu, S., Wisniewski, D., Evans, J. F., and Soberman, R. J. (2004) The membrane organization of leukotriene synthesis. *Proc. Natl. Acad. Sci. U.S.A. 101*, 6587–6592.
54. Ruan, K. H., Deng, H., and So, S. P. (2006) Engineering of a protein with cyclooxygenase and prostacyclin synthase activities that converts arachidonic acid to prostacyclin. *Biochemistry 45*, 14003–14011.
55. Farmaki, T., Sanmartin, M., Jimenez, P., Paneque, M., Sanz, C., Vancanneyt, G., Leon, J., and Sanchez-Serrano, J. J. (2007) Differential distribution of the lipoxygenase pathway enzymes within potato chloroplasts. *J. Exp. Bot. 58*, 555–568.
56. Cook, A. C., Ho, C., Kershner, J. L., Malinowski, S. A., Moldveen, H., Stagliano, B. A., and Slater, S. J. (2006) Competitive binding of protein kinase Calpha to membranes and Rho GTPases. *Biochemistry 45*, 14452–14465.

BI800751P